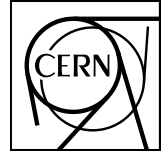




Light vector meson production in pp collisions at $\sqrt{s} = 7$ TeV



CERN-PH-EP-2011-196
27 November 2011

Light vector meson production in pp collisions at $\sqrt{s} = 7$ TeV

The ALICE Collaboration*

Abstract

The ALICE experiment has measured low-mass dimuon production in pp collisions at $\sqrt{s} = 7$ TeV in the dimuon rapidity region $2.5 < y < 4$. The observed dimuon mass spectrum is described as a superposition of resonance decays ($\eta, \rho, \omega, \eta', \phi$) into muons and semi-leptonic decays of charmed mesons. The measured production cross sections for ω and ϕ are $\sigma_{\omega}(1 < p_t < 5 \text{ GeV}/c, 2.5 < y < 4) = 5.28 \pm 0.54(\text{stat}) \pm 0.50(\text{syst}) \text{ mb}$ and $\sigma_{\phi}(1 < p_t < 5 \text{ GeV}/c, 2.5 < y < 4) = 0.940 \pm 0.084(\text{stat}) \pm 0.078(\text{syst}) \text{ mb}$. The differential cross sections $d^2\sigma/dydp_t$ are extracted as a function of p_t for ω and ϕ . The ratio between the ρ and ω cross section is obtained. Results for the ϕ are compared with other measurements at the same energy and with predictions by models.

arXiv:1112.2222v1 [nucl-ex] 9 Dec 2011

*See Appendix A for the list of collaboration members

1 Introduction

The measurement of light vector meson production (ρ, ω, ϕ) in pp collisions provides insight into soft Quantum Chromodynamics (QCD) processes in the LHC energy range. Calculations in this regime are based on QCD inspired phenomenological models [1] that must be tuned to the data, in particular for hadrons that contain the u, d, s quarks. The evolution of particle production as a function of \sqrt{s} is difficult to establish. Measurements at mid-rapidity in pp collisions at the beam injection energy of the LHC ($\sqrt{s} = 0.9$ TeV) were performed by the ALICE experiment [2], and compared with several PYTHIA [3] tunes and PHOJET [4]. The comparison showed that, for transverse momenta larger than ~ 1 GeV/ c , the strange particle spectra are strongly underestimated by the models, by a factor of 2 for K_S^0 and 3 for hyperons, with a smaller discrepancy for the ϕ . Extending the measurements to larger energies and complementary rapidity domains is needed in order to further constrain the models.

Moreover, light vector meson production provides a reference for high-energy heavy-ion collisions. In fact, key information on the hot and dense state of strongly interacting matter produced in these collisions can be extracted measuring light meson production.

The ALICE experiment at the LHC can access vector mesons produced in the rapidity range $2.5 < y < 4$ through their decays into muon pairs ¹. In this Letter we report results obtained in pp collisions at $\sqrt{s} = 7$ TeV in the dimuon transverse momentum range $1 < p_t < 5$ GeV/ c based on the full data sample collected in 2010 with a minimum bias muon trigger. The measurement is done via a combined fit of the dimuon invariant mass spectrum after combinatorial background subtraction.

2 Experimental setup

The ALICE detector is fully described elsewhere [5]. The main detectors relevant for this analysis are the forward muon spectrometer, which covers the pseudo-rapidity region $-4 < \eta < -2.5$, the VZERO detector and the Silicon Pixel Detector (SPD) of the Inner Tracking System.

The elements of the muon spectrometer are a front hadron absorber, followed by a set of tracking stations, a dipole magnet, an iron wall acting as muon filter and a trigger system.

The front hadron absorber is made of carbon, concrete and steel and is placed at a distance of 0.9 m from the nominal interaction point (IP). Its total length of material corresponds to ten hadronic interaction lengths. The dipole magnet is 5 m long and provides a magnetic field of up to 0.7 T in the vertical direction which gives a field integral of 3 Tm.

The muon tracking is provided by a set of five tracking stations, each one composed of two cathode pad chambers. The stations are located between 5.2 and 14.4 m from the IP, the first two upstream of the dipole magnet, the third in the middle of the dipole magnet gap and the last two downstream. The intrinsic spatial resolution of the tracking chambers is ~ 100 μm in the bending direction.

A 1.2 m thick iron wall, corresponding to 7.2 hadronic interaction lengths, is placed between the tracking and trigger systems and absorbs the residual secondary hadrons emerging from the front absorber. The front absorber together with the muon filter stops muons with momentum lower than 4 GeV/ c . The muon trigger system consists of two detector stations, placed at 16.1 and 17.1 m from the IP. Each one is composed of two planes of resistive plate chambers (RPC), with a time resolution of about 2 ns.

The SPD consists of two cylindrical layers of silicon pixel detectors, positioned at a radius of 3.9 and 7.6 cm from the beam. The pseudo-rapidity range covered by the inner and the outer layer is $|\eta| < 2.0$ and $|\eta| < 1.6$, respectively. Besides contributing to the primary vertex determination, it is used for the

¹In the ALICE coordinates, the muon spectrometer covers the pseudo-rapidity range $-4 < \eta < -2.5$, where the z axis is oriented along the beam direction. However, since in pp collisions results are symmetric with respect to $y = 0$, we prefer to drop the negative sign when quoting the rapidity values.

input of the level-0 trigger (L0).

The VZERO detector consists of two arrays of plastic scintillators placed at 3.4 m and -0.9 m from the IP and covering the pseudo-rapidity regions $2.8 < \eta < 5.1$ and $-3.7 < \eta < -1.7$, respectively. This detector provides timing information for the L0 trigger and has a time resolution better than 1 ns, thus giving the possibility to reject beam-halo and beam-gas interactions in the off-line analysis.

3 Data selection and analysis

During the pp run in 2010, the instantaneous luminosity delivered by the LHC to ALICE ranged from 0.6×10^{29} to $1.2 \times 10^{30} \text{cm}^{-2} \text{s}^{-1}$. The fraction of events with multiple interactions in a single bunch crossing was less than 5%. The data sample used in this analysis was collected using the muon trigger, which is activated when at least three of the four RPC planes in the two muon trigger stations give a signal compatible with a track in the muon trigger system. To evaluate the integrated luminosity (\mathcal{L}_{int}), a minimum bias (MB) trigger, independent of the muon trigger, was collected in parallel. It is activated when at least one out of the 1200 SPD readout chips detects a hit or when at least one of the two VZERO scintillator arrays has fired, in coincidence with the arrival of bunches from both sides.

The integrated luminosity was determined by measuring the MB cross section σ_{MB} and counting the number of MB events. The σ_{MB} value is 62.3 mb, and is affected by a 4% systematic uncertainty. It was obtained measuring the cross section σ_{V0AND} [6], for the occurrence of coincident signals in the two VZERO detectors (V0AND) in a van der Meer scan [7]. The factor $\sigma_{\text{V0AND}}/\sigma_{\text{MB}}$ was obtained as the fraction of MB events where the L0 trigger input corresponding to the V0AND condition has fired. Its value is 0.87 and is stable within 0.5% over the analyzed data. The full data sample used for this analysis, amounting to an integrated luminosity of approximately 85nb^{-1} , was used to extract the p_t distributions. Part of the data was not collected with the MB trigger in parallel with the muon trigger. For this fraction, the integrated luminosity could not be measured and the ω and ϕ cross sections were determined with the remaining subsample corresponding to $\mathcal{L}_{\text{int}} = 55.7 \text{nb}^{-1}$.

Track reconstruction in the muon spectrometer is based on a Kalman filter algorithm [8, 9]. Straight line segments are formed from the clusters on the two planes of each of the most downstream tracking stations (4 and 5), since these are less affected by the background coming from soft particles that emerge from the front absorber. Track properties are first estimated assuming that tracks originate from the IP and are bent in a uniform magnetic field in the dipole. Afterwards, track candidates starting in station 4 are extrapolated to station 5, or vice versa, and paired with at least one cluster on the basis of a χ^2 cut. Parameters are then recalculated using the Kalman filter. The same procedure is applied to the upstream stations, rejecting track candidates that cannot be matched to a cluster in the acceptance of the spectrometer. Finally, fake tracks that share the same cluster with other tracks are removed and a correction for energy loss and multiple Coulomb scattering in the absorber is applied by using the Branson correction [8]. The relative momentum resolution of the reconstructed tracks ranges from 1% at 20 GeV/c to 4% at 100 GeV/c.

Muons were selected requiring that the direction and position of each muon track reconstructed in the tracking chambers match the ones of the corresponding track in the trigger stations. A cut on the muon rapidity $2.5 < y_\mu < 4$ was applied in order to remove the tracks close to the acceptance borders. Muon pairs were selected requiring that both muons satisfy these cuts. Approximately 291,000 opposite-sign (N_{+-}) and 197,000 like-sign (N_{++} , N_{--}) muon pairs passed these selections.

The opposite-sign pairs are composed of correlated and uncorrelated pairs. The former constitute the signal, while the latter, coming mainly from decays of pions and kaons into muons, form the combinatorial background, which was evaluated using an event mixing technique. The distribution obtained was normalized to $2R\sqrt{N_{++}N_{--}}$, where N_{++} (N_{--}) is the number of like-sign positive (negative) pairs

integrated in the full mass range. It is assumed that the like-sign pairs are uncorrelated. The fraction of correlated like-sign pairs, coming from the decay chain of beauty mesons and $B - \bar{B}$ oscillations [10] was determined from the measured open charm content and the ratio between open beauty and charm (see below). It amounts to $\approx 0.5\%$ for $p_t > 1$ GeV/c and $M < 1.5$ GeV/c², and was thus neglected. The R factor is defined as $A_{+-}/\sqrt{A_{++}A_{--}}$, where A_{++} (A_{--}) is the acceptance for a $++$ ($--$) pair, and takes into account possible correlations introduced by the detector. It was evaluated using two methods. The first employs MC simulations to determine the acceptances $A_{\pm\pm}$. The other method uses the mixed-event pairs to estimate R as $R = N_{+-}^{\text{mixed}}/\sqrt{N_{++}^{\text{mixed}}N_{--}^{\text{mixed}}}$, where $N_{\pm\pm}^{\text{mixed}}$ is the number of mixed pairs for a given charge combination. The two methods are in agreement for $p_t > 1$ GeV/c. We obtain $R = 0.95$ for $p_t > 1$ GeV/c. The event mixing procedure was cross-checked by comparing the results obtained for like-sign mixed pairs with the non-mixed ones. The shapes are identical, while the number of like-sign pairs estimated with the event mixing is lower than the one in the data by 5%. We take this value as the systematic uncertainty on the background normalization. The signal-to-background ratio for $p_t > 1$ GeV/c is about 1 at the ϕ and ω masses. Alternatively, the combinatorial background can be evaluated using only the like-sign pairs in the non-mixed data, and calculating for each ΔM mass bin the quantity $2R(\Delta M)\sqrt{N_{++}(\Delta M)N_{--}(\Delta M)}$. Figure 1 shows the invariant mass spectrum for opposite sign muon pairs in different p_t ranges, together with the combinatorial background estimated with the event mixing technique or using the like-sign pairs. It is seen that the two techniques are in good agreement for $p_t > 1$ GeV/c. For lower pair transverse momenta both methods fail in describing the background. In this region, the method based on the like-sign pairs gives a background mass spectrum that overshoots the opposite-sign pair spectrum, while the event mixing technique does not reproduce the non-mixed like-sign pairs spectra. The analysis is thus limited to $p_t > 1$ GeV/c. The event mixing technique is used, since it is less affected by statistical fluctuations.

After subtracting the combinatorial background from the opposite-sign mass spectrum, we obtain the raw signal mass spectrum shown in Fig. 2. The mass resolution at the ϕ mass is $\sigma_M \approx 60$ MeV/c², in good agreement with the Monte Carlo simulation. The processes contributing to the dimuon mass spectrum are the light meson (η , ρ , ω , η' , ϕ) decays into muons and the correlated semi-leptonic open charm and beauty decays. The light meson contributions were obtained performing a simulation based on a hadronic cocktail generator. The input rapidity distributions for all particles are based on a parametrization of PYTHIA 6.4 [3] results obtained with the Perugia-0 tune [11]. The same procedure is followed for the η' p_t distribution, while for ρ , ω and ϕ the transverse momentum is described with a power-law function, used also by the HERA-B experiment to fit the ϕ p_t^2 spectrum [12]:

$$\frac{dN}{dp_t} = C \frac{p_t}{[1 + (p_t/p_0)^2]^n}. \quad (1)$$

The parameters n and p_0 were tuned iteratively to the results of this analysis. The p_t distribution of η is based on preliminary results from η production yields measured in the two-photon decay channel by ALICE [13]. The open charm and beauty generation is based on a parameterization of PYTHIA [8]. The detector response for all these processes is obtained with a simulation that uses the GEANT3 [14] transport code. The simulation results are then subjected to the same reconstruction and selection chain as the real data. The invariant mass spectrum is fitted with a superposition of the aforementioned contributions. The free parameters of the fit are the normalizations of the $\eta \rightarrow \mu\mu\gamma$, $\omega \rightarrow \mu\mu$, $\phi \rightarrow \mu\mu$ and open charm signals. The processes $\eta \rightarrow \mu\mu$ and $\omega \rightarrow \mu\mu\pi^0$ are fixed according to the relative branching ratios. The contribution from $\rho \rightarrow \mu\mu$ was fixed by the assumption that the production cross section of ρ and ω are equal [15, 16, 17]. The η' contribution was set fixing the ratio between the η' and η cross sections according to PYTHIA. The ratio between the open beauty and open charm was fixed according to the results from the LHCb Collaboration [18, 19]. The main sources of systematic uncertainty are the background normalization and the relative normalization of the sources, mainly due to the error on the branching ratios for the ω and η' Dalitz decays. The raw numbers of ϕ and $\rho + \omega$ resonances obtained from the fit are $N_{\phi}^{\text{raw}} = (3.20 \pm 0.15) \times 10^3$ and $N_{\rho+\omega}^{\text{raw}} = (6.83 \pm 0.15) \times 10^3$.

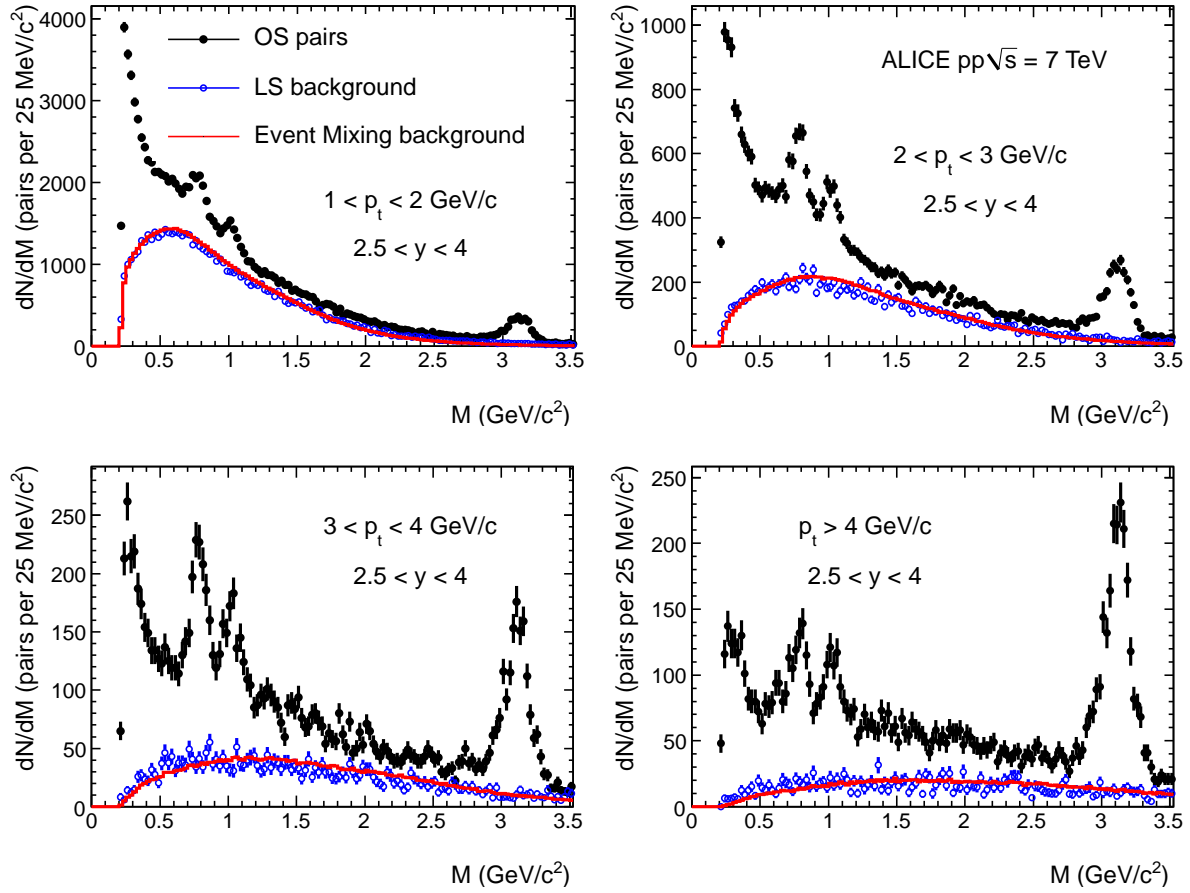


Figure 1: (Color online) Invariant mass spectra for opposite-sign muon pairs in pp at $\sqrt{s} = 7$ TeV in different p_t ranges. The combinatorial background, evaluated from opposite-sign pairs in mixed events (red line) or like-sign pairs in non-mixed events (blue points), is also shown.

4 Results

The ϕ production cross section was evaluated in the range $2.5 < y < 4$, $1 < p_t < 5$ GeV/c through the formula:

$$\sigma_\phi = \frac{N_\phi^{\text{raw}}}{A_\phi \varepsilon_\phi BR(\phi \rightarrow l^+ l^-)} \frac{\sigma_{MB}}{N_{MB}} \frac{N_\mu^{MB}}{N_\mu^{\mu-MB}},$$

where N_ϕ^{raw} is the measured number of ϕ mesons, A_ϕ and ε_ϕ are the geometrical acceptance and the efficiency respectively, N_{MB} is the number of minimum bias collisions, σ_{MB} is the ALICE minimum bias cross section in pp collisions at $\sqrt{s} = 7$ TeV, and $N_\mu^{MB}/N_\mu^{\mu-MB}$ is the ratio between the number of single muons collected with the minimum bias trigger and with the muon trigger in the region $2.5 < y_\mu < 4$, $p_t > 1$ GeV/c. The number of minimum bias collisions was corrected, as a function of time, by the probability to have multiple interactions in a single bunch crossing. Finally, $BR(\phi \rightarrow l^+ l^-) = (2.95 \pm 0.03) \times 10^{-4}$ is the branching ratio into lepton pairs. Assuming lepton universality, this number is obtained as a weighted mean of the measured branching ratio in $\mu^+ \mu^-$ with that into $e^+ e^-$, because the latter has a much smaller experimental uncertainty than the former [20]. The number of ϕ mesons was evaluated by performing a fit to the mass spectrum for each $\Delta p_t = 0.5$ GeV/c interval in the transverse momentum range covered by the analysis. The acceptance-corrected results were then summed in order to obtain the total number of ϕ mesons. In this way the dependence of the acceptance correction on the input p_t distribution used for the Monte Carlo simulation becomes insignificant. Alternatively, a fit was performed on the mass spectrum integrated over $1 < p_t < 5$ GeV/c and a global correction factor was applied. The results of

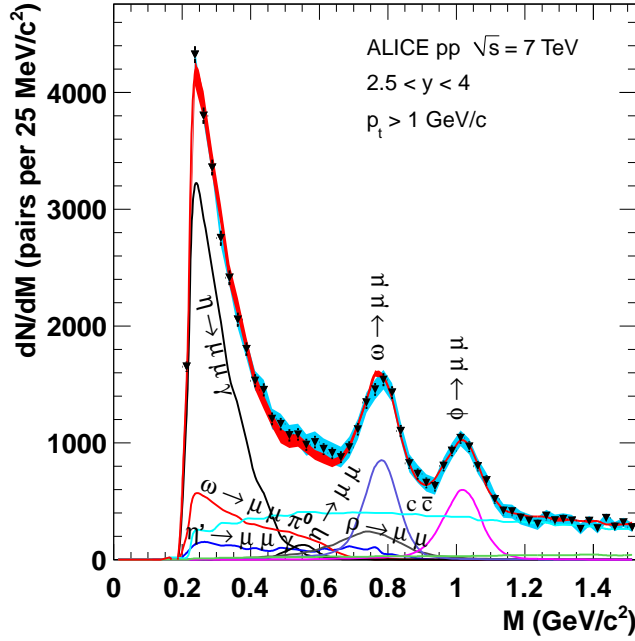


Figure 2: (Color online) Dimuon invariant mass spectrum in pp at $\sqrt{s} = 7$ TeV after combinatorial background subtraction for $p_t > 1$ GeV/c (triangles). Light blue band: systematic uncertainty from background subtraction. Red band: sum of all simulated contributions. The width of the red band represents the uncertainty on the relative normalization of the sources.

the two approaches agree within 3%. The first approach was used for the results reported in this paper. The ϕ meson acceptance and efficiency correction in the range covered by this analysis was evaluated through Monte Carlo simulations and ranges from 10% to 13%, depending on the data-taking period. The ratio $N_\mu^{MB}/N_\mu^{\mu-MB}$ strongly depends on the data taking conditions and was evaluated as a function of time.

We obtain $\sigma_\phi(1 < p_t < 5 \text{ GeV}/c, 2.5 < y < 4) = 0.940 \pm 0.084(\text{stat}) \pm 0.078(\text{syst}) \text{ mb}$. The systematic uncertainty results from the uncertainty on the background subtraction (2%), the ϕ branching ratio into dileptons (1%), the muon trigger and tracking efficiency (4% and 3% respectively), the minimum bias cross section (4%) and the ratio $N_\mu^{MB}/N_\mu^{\mu-MB}$ (3%). The first two contributions have been described above. The others are common to all analyses in the dimuon channel, and are extensively discussed elsewhere [21]. Here, only the main points are briefly summarized. The muon trigger efficiency was estimated measuring the number of J/ψ mesons decaying into muons, after efficiency and acceptance corrections, in two ways: in the first case both muons were required to match the trigger, while in the second only one muon needed to fulfill this condition. The tracking efficiency was evaluated starting from the determination of the efficiency for individual chambers, computed by taking advantage from the redundancy of the tracking information in each station. The same procedure was applied to the data and to the Monte Carlo simulations. The differences in the results give the systematic uncertainty on the tracking efficiency. The error on the minimum bias cross section is mainly due to the uncertainties in the beam intensities [22] and in the analysis procedure adopted for the determination of the beam luminosity via the van der Meer scan. The error on the ratio $N_\mu^{MB}/N_\mu^{\mu-MB}$ was evaluated comparing the value measured as described above with the information obtained from the trigger scalers, taking into account the dead time of the triggers [23].

Table 1 compares the present measurement with some commonly used tunes of PYTHIA [3] (Perugia-0 [11], Perugia-11 [24], ATLAS-CSC [25] and D6T [26]) and PHOJET [4]. It can be seen that Perugia-0

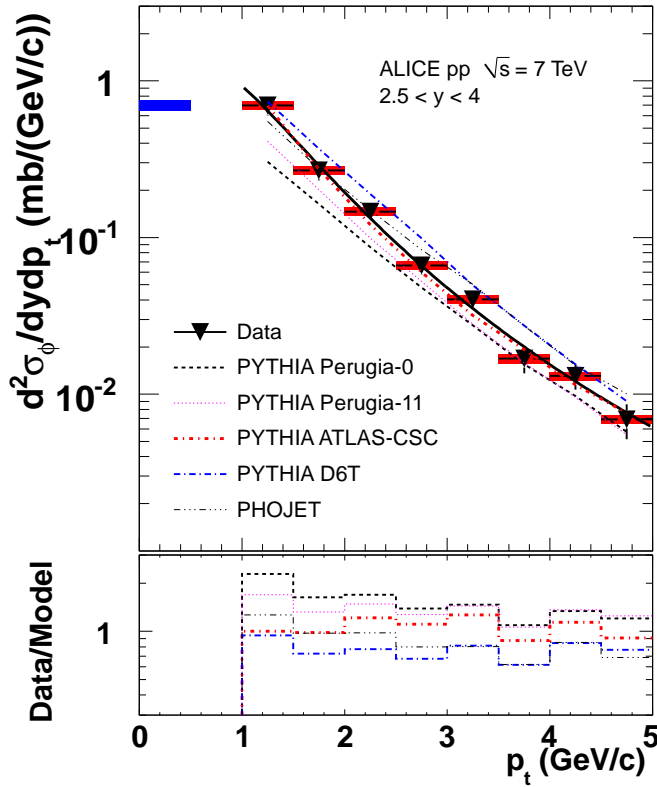


Figure 3: Top: Inclusive differential ϕ production cross section $d^2\sigma_\phi/dydp_t$ for $2.5 < y < 4$. The error bars represent the quadratic sum of the statistical and systematic uncertainties, the red boxes the point-to-point uncorrelated systematic uncertainty, the blue box on the left the error on normalization. Data are fitted with Eq. (1) (solid line) and compared with the Perugia-0, Perugia-11, ATLAS-CSC and D6T PYTHIA tunes and with PHOJET. Bottom: Ratio between data and models.

and Perugia-11 underestimate the ϕ cross section (by about a factor of 2 and 1.5, respectively), while the others agree with the measurement within its error.

The differential cross section $d^2\sigma_\phi/dydp_t$ is shown in Fig. 3 (top). Numerical values are reported in Table 2. p_t -dependent contributions to the systematic uncertainties, due to the uncertainty on trigger and tracking efficiency and background subtraction, are indicated as red boxes. The uncertainty on the minimum bias cross section, branching ratio and $N_\mu^{MB}/N_\mu^{\mu-MB}$ ratio contribute to the uncertainty in the overall normalization. As stated above, the ϕ cross section is extracted from a subsample of the data used to determine the p_t distribution, and is thus affected by a larger statistical uncertainty, resulting in a 5% contribution to the normalization error. Fitting the expression in Eq. (1) (solid line) to the differential cross section gives $p_0 = 1.16 \pm 0.23 \text{ GeV}/c$ and $n = 2.7 \pm 0.2$. The PYTHIA and PHOJET predictions are also displayed in Fig. 3, where the bottom panel shows the ratio between the measurement and the model predictions. PYTHIA with the ATLAS-CSC and D6T tunes reproduces the measured differential cross section, while the others predict a harder p_t spectrum.

The results are compared to measurements of $\phi \rightarrow K^+K^-$ for $2.44 < y < 4.06$ by the LHCb Collaboration [27] in Fig. 4. The observed shapes of the p_t distributions are similar. In order to compare with our integrated cross section result, the differential cross section measurement by LHCb was integrated for $p_t > 1 \text{ GeV}/c$ and scaled by a small correction factor, obtained from PYTHIA (Perugia-0), to account for the slight difference in rapidity acceptance. The result is $\sigma_\phi = 1.07 \pm 0.15(\text{stat.} + \text{syst.}) \text{ mb}$. When the statistical errors and the part of the systematic uncertainty which is not correlated among the two

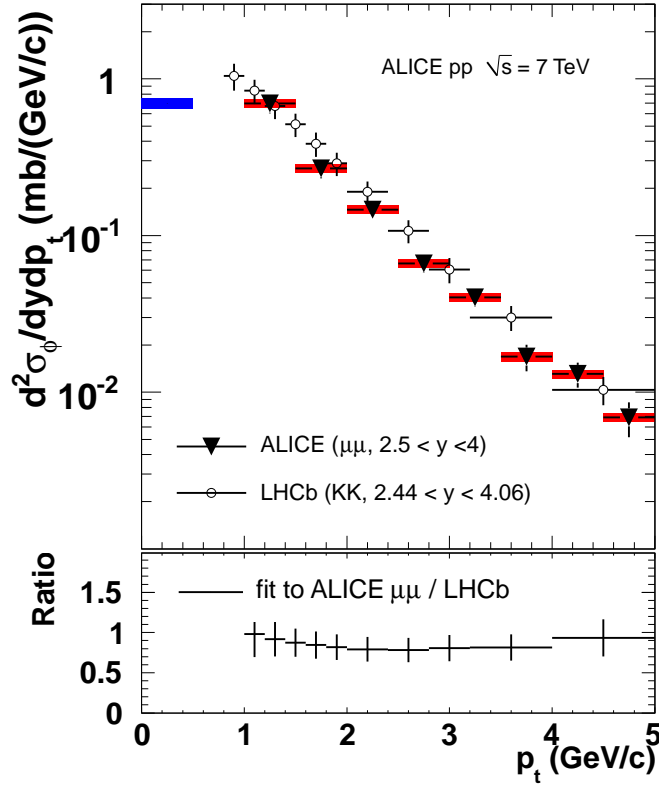


Figure 4: (Color online) Top: Inclusive differential ϕ production cross section $d^2\sigma_\phi/dydp_t$, as measured via the decay into dimuons (black triangles). The blue box on the left represents the error on normalization. The data are compared to the measurements in the kaon decay channel by LHCb (black open circles) [27]. Bottom: Fit to the differential cross section measured in dimuons divided by the cross section measured in the kaon channel by LHCb.

experiments are properly taken into account, the two measurements are in agreement.

The ratio $N_\phi/(N_\rho + N_\omega) = BR(\phi \rightarrow \mu\mu)\sigma_\phi/[BR(\rho \rightarrow \mu\mu)\sigma_\rho + BR(\omega \rightarrow \mu\mu)\sigma_\omega]$, corrected for acceptance and efficiency, was calculated for $1 < p_t < 5$ GeV/c , giving $0.416 \pm 0.032(\text{stat.}) \pm 0.004(\text{syst.})$. Systematic uncertainties are due to the normalizations of $\omega \rightarrow \mu\mu\pi^0$, $\eta' \rightarrow \mu\mu\gamma$ and combinatorial background. The corresponding ratio is calculated with PYTHIA and PHOJET. All the predictions underestimate the measured ratio, as reported in Table 1. The p_t dependence of this ratio is shown in Fig. 5. The Perugia-0, Perugia-11 and D6T tunes systematically underestimate this ratio, while PHOJET correctly reproduces the data for $p_t > 3$ GeV/c , and ATLAS-CSC is in agreement with the measurement for $p_t > 1.5$ GeV/c .

In order to extract the ω cross section, the ρ and ω contributions must be disentangled, leaving the ρ normalization as an additional free parameter in the fit to the dimuon mass spectrum. The result of the fit for $1 < p_t < 5$ GeV/c gives $\sigma_\rho/\sigma_\omega = 1.15 \pm 0.20(\text{stat}) \pm 0.12(\text{syst})$, in agreement with model predictions, as shown in Table 1. The systematic uncertainty was evaluated changing the normalizations of the $\eta' \rightarrow \mu\mu\gamma$ and $\omega \rightarrow \mu\mu\pi^0$ according to the uncertainties in their branching ratios and the background level by $\pm 10\%$, which corresponds to twice the uncertainty in the normalization. The ω production cross section, calculated from this ratio, is $\sigma_\omega(1 < p_t < 5 \text{ GeV}/c, 2.5 < y < 4) = 5.28 \pm 0.54(\text{stat}) \pm 0.50(\text{syst})$ mb. This value is in agreement with the Perugia-0 PYTHIA tune, while the other tunes and PHOJET overestimate the ω cross section, as shown in Table 1.

In Fig. 6 (top) the ω differential cross section is shown. Numerical values are reported in Table 2. A fit

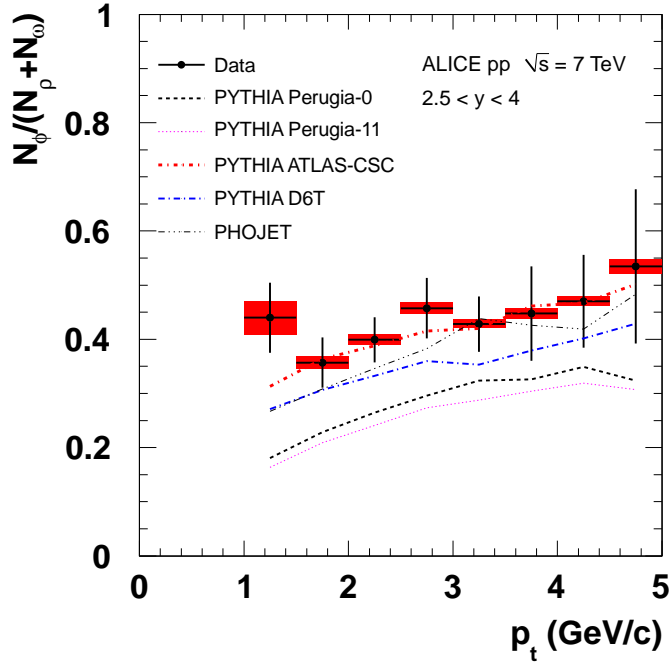


Figure 5: Ratio $N_\phi/(N_\rho + N_\omega)$ as a function of the dimuon transverse momentum.

Table 1: Measured cross sections and ratios compared to the calculation from PYTHIA with several tunes and PHOJET in the range $1 < p_t < 5$ GeV/c, $2.5 < y < 4$

	σ_ϕ (mb)	σ_ω (mb)	$\frac{N_\phi}{N_\rho + N_\omega}$	$\sigma_\rho/\sigma_\omega$
ALICE $\mu\mu$ measurement	$0.940 \pm 0.084 \pm 0.078$	$5.28 \pm 0.54 \pm 0.50$	$0.416 \pm 0.032 \pm 0.004$	$1.15 \pm 0.20 \pm 0.12$
PYTHIA/Perugia-0	0.50	5.60	0.22	1.03
PYTHIA/Perugia-11	0.62	7.81	0.20	1.03
PYTHIA/ATLAS-CSC	0.91	6.50	0.35	1.05
PYTHIA/D6T	1.12	9.15	0.30	1.04
PHOJET	0.87	6.89	0.30	1.08

of Eq. (1) (solid line) to the data gives $p_0 = 1.44 \pm 0.09$ GeV/c and $n = 3.2 \pm 0.1$. As shown in the same figure (bottom), all the PYTHIA tunes reproduce the p_t slope, while PHOJET gives a slightly harder spectrum.

5 Conclusions

Vector meson production in pp collisions at $\sqrt{s} = 7$ TeV was measured through the dimuon decay channel in $2.5 < y < 4$ and $p_t > 1$ GeV/c. The inclusive ϕ production cross section $\sigma_\phi(1 < p_t < 5$ GeV/c, $2.5 < y < 4) = 0.940 \pm 0.084(\text{stat}) \pm 0.078(\text{syst})$ mb was measured with a sample corresponding to an integrated luminosity $\mathcal{L}_{\text{int}} = 55.7$ nb $^{-1}$. Calculations based on PHOJET and PYTHIA with the ATLAS-CSC and D6T tunes give results that are in agreement with the measurement, while the Perugia-0 and Perugia-11 PYTHIA tunes underestimate the cross section by about a factor of 2 and 1.5, respectively. The ratio $N_\phi/(N_\rho + N_\omega)$, calculated for $1 < p_t < 5$ GeV/c, gives $0.416 \pm 0.032 \pm 0.004$. This value is reproduced by PHOJET for $p_t > 3$ GeV/c, and by the ATLAS-CSC tune for $p_t > 1.5$ GeV/c, while the other tunes underestimate the ratio in the full range $1 < p_t < 5$ GeV/c. By measuring the ratio of the ρ and ω cross sections, $\sigma_\rho/\sigma_\omega = 1.15 \pm 0.20(\text{stat}) \pm 0.12(\text{syst})$, it was possible to extract the inclusive ω production cross section $\sigma_\omega(1 < p_t < 5$ GeV/c, $2.5 < y < 4) = 5.28 \pm 0.54(\text{stat}) \pm 0.50(\text{syst})$ mb. While all models correctly reproduce the measured $\sigma_\rho/\sigma_\omega$ ratio, the ω cross section is correctly reproduced only by the

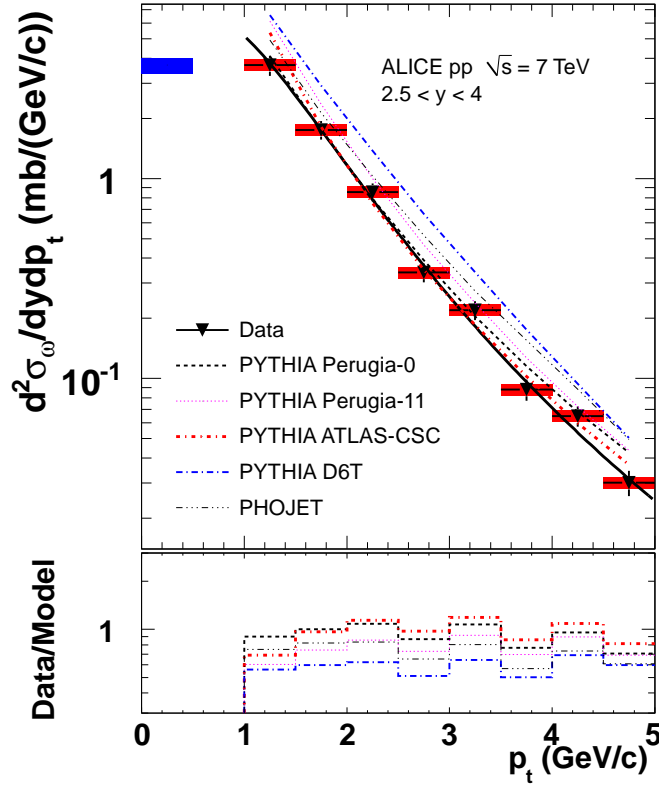


Figure 6: (Color online) Top: Inclusive differential ω production cross section $d^2\sigma_\omega/dydp_t$ for $2.5 < y < 4$. The error bars represent the quadratic sum of the statistical and systematic uncertainties, the red boxes the point-to-point uncorrelated systematic uncertainty, the blue box on the left the error on normalization. Data are fitted with Eq. (1) (solid line) and compared with the Perugia-0, Perugia-11, ATLAS-CSC and D6T PYTHIA tunes and PHOJET. Bottom: Ratio between data and models.

Table 2: ϕ and ω differential cross sections for $2.5 < y < 4$. Statistical, bin-to-bin uncorrelated and correlated systematic errors are reported.

p_t (GeV/c)	$d^2\sigma_\phi/dydp_t$ (mb/(GeV/c))	$d^2\sigma_\omega/dydp_t$ (mb/(GeV/c))
[1, 1.5]	$0.695 \pm 0.079 \pm 0.046 \pm 0.053$	$3.69 \pm 0.35 \pm 0.24 \pm 0.32$
[1.5, 2]	$0.268 \pm 0.032 \pm 0.018 \pm 0.020$	$1.75 \pm 0.15 \pm 0.12 \pm 0.15$
[2, 2.5]	$0.147 \pm 0.014 \pm 0.010 \pm 0.011$	$0.857 \pm 0.069 \pm 0.057 \pm 0.075$
[2.5, 3]	$0.0665 \pm 0.0074 \pm 0.0044 \pm 0.0051$	$0.339 \pm 0.029 \pm 0.022 \pm 0.030$
[3, 3.5]	$0.0403 \pm 0.0044 \pm 0.0027 \pm 0.0031$	$0.220 \pm 0.019 \pm 0.011 \pm 0.019$
[3.5, 4]	$0.0169 \pm 0.0031 \pm 0.0011 \pm 0.0013$	$0.0880 \pm 0.0088 \pm 0.0058 \pm 0.0077$
[4, 4.5]	$0.0131 \pm 0.0022 \pm 0.0009 \pm 0.0010$	$0.0648 \pm 0.0062 \pm 0.0043 \pm 0.0056$
[4.5, 5]	$0.0069 \pm 0.0017 \pm 0.0005 \pm 0.0005$	$0.0301 \pm 0.0039 \pm 0.0020 \pm 0.0026$

Perugia-0 calculation, and overestimated by the others. The differential production cross sections of ω and ϕ were measured. The p_t dependence of the ϕ cross section agrees well with other measurements done in the kaon decay channel. The ATLAS-CSC and D6T tunes correctly reproduce the ϕ p_t spectrum, while the other calculations predict harder spectra. PHOJET predicts also a slightly harder p_t spectrum for the ω , while PYTHIA provides slopes which are closer to the one obtained with this measurement.

References

- [1] T. Sjöstrand, P.Z. Skands, Eur. Phys. J. **C39** (2005) 129.

- [2] K. Aamodt *et al.* (ALICE Collaboration), *Eur. Phys. J.* **C71** (2011) 1594.
- [3] T. Sjöstrand *et al.*, *J. High Energy Phys.* **05** (2006) 026.
- [4] R. Engel *et al.*, *Z. Phys.* **C66** (1995) 203; R. Engel and J. Ranft, *Phys. Rev.*
- [5] K. Aamodt *et al.* (ALICE Collaboration), *JINST* **3** (2008) S08002.
- [6] M. Gagliardi *et al.* (ALICE Collaboration), proceedings of the International Workshop on Early Physics with Heavy-Ion Collisions at LHC, July 6th – 8th 2011, Bari (Italy).
- [7] S. van der Meer, ISR-PO/68-31, KEK68-64.
- [8] L. Aphecetche *et al.*, ALICE Internal Note ALICE-INT-2009-044, <https://edms.cern.ch/document/1054937/1>.
- [9] G. Chabratova *et al.*, ALICE Internal Note ALICE-INT-2003-002, <https://edms.cern.ch/document/371480/1>.
- [10] P. Braun-Munzinger, P. Crochet, *Nucl. Instr. Meth. Phys. Res.* **A484** (2002) 564.
- [11] P.Z. Skands, arXiv: 0905.3418 (2009).
- [12] I. Abt *et al.* (HERA-B Collaboration), *Eur. Phys. J.* **C50** (2007) 315.
- [13] K. Reyers *et al.* (ALICE Collaboration), *J. Phys.* **G38** (2011) 124076.
- [14] R. Brun *et al.*, CERN Program Library Long Write-up, W5013, GEANT3 Detector Description and Simulation Tool, 1994.
- [15] M. Aguilar-Benitez *et al.*, *Z. Phys.* **C50** (1991) 405.
- [16] G. Agakichiev *et al.* (CERES Collaboration), *Eur. Phys. J.* **C4** (1998) 231.
- [17] A. Uras *et al.* (NA60 Collaboration), *J. Phys.* **G38** (2011) 124180.
- [18] LHCb Collaboration, "Prompt charm production in pp collisions at $\sqrt{s} = 7$ TeV", CERN-LHCb-CONF-2010-013 (2010) unpublished.
- [19] R. Aaij *et al.* (LHCb Collaboration), *Phys. Lett.* **B694** (2010) 209.
- [20] K. Nakamura *et al.* (Particle Data Group), *J. Phys.* **G37** (2010) 075021.
- [21] K. Aamodt *et al.* (ALICE Collaboration), *Phys. Lett.* **B704** (2011) 442.
- [22] G. Anders *et al.*, CERN-ATS-Note-2011-016 PERF.
- [23] L. Aphecetche *et al.*, ALICE-SCIENTIFIC-NOTE-2011-001, <http://cdsweb.cern.ch/record/1388921>.
- [24] P.Z. Skands, *Phys. Rev.* **D82** (2010) 074018.
- [25] C. Buttar *et al.*, *Acta Phys. Pol.* **B35** (2004) 433.
- [26] R. Field, *Acta Phys. Pol.* **B39** (2008) 2611 and arXiv: 1003.4220 (2010). **D54** (1996) 4244.
- [27] R. Aaij *et al.* (LHCb Collaboration), *Phys.Lett.* **B703** (2011) 267.

6 Acknowledgements

The ALICE collaboration would like to thank all its engineers and technicians for their invaluable contributions to the construction of the experiment and the CERN accelerator teams for the outstanding performance of the LHC complex.

The ALICE collaboration acknowledges the following funding agencies for their support in building and running the ALICE detector:

Department of Science and Technology, South Africa;

Calouste Gulbenkian Foundation from Lisbon and Swiss Fonds Kidagan, Armenia;

Conselho Nacional de Desenvolvimento Científico e Tecnológico (CNPq), Financiadora de Estudos e Projetos (FINEP), Fundação de Amparo à Pesquisa do Estado de São Paulo (FAPESP);

National Natural Science Foundation of China (NSFC), the Chinese Ministry of Education (CMOE) and the Ministry of Science and Technology of China (MSTC);

Ministry of Education and Youth of the Czech Republic;
 Danish Natural Science Research Council, the Carlsberg Foundation and the Danish National Research Foundation;
 The European Research Council under the European Community's Seventh Framework Programme;
 Helsinki Institute of Physics and the Academy of Finland;
 French CNRS-IN2P3, the 'Region Pays de Loire', 'Region Alsace', 'Region Auvergne' and CEA, France;
 German BMBF and the Helmholtz Association;
 General Secretariat for Research and Technology, Ministry of Development, Greece;
 Hungarian OTKA and National Office for Research and Technology (NKTH);
 Department of Atomic Energy and Department of Science and Technology of the Government of India;
 Istituto Nazionale di Fisica Nucleare (INFN) of Italy;
 MEXT Grant-in-Aid for Specially Promoted Research, Japan;
 Joint Institute for Nuclear Research, Dubna;
 National Research Foundation of Korea (NRF);
 CONACYT, DGAPA, México, ALFA-EC and the HELEN Program (High-Energy physics Latin-American-European Network);
 Stichting voor Fundamenteel Onderzoek der Materie (FOM) and the Nederlandse Organisatie voor Wetenschappelijk Onderzoek (NWO), Netherlands;
 Research Council of Norway (NFR);
 Polish Ministry of Science and Higher Education;
 National Authority for Scientific Research - NASR (Autoritatea Națională pentru Cercetare Științifică - ANCS);
 Federal Agency of Science of the Ministry of Education and Science of Russian Federation, International Science and Technology Center, Russian Academy of Sciences, Russian Federal Agency of Atomic Energy, Russian Federal Agency for Science and Innovations and CERN-INTAS;
 Ministry of Education of Slovakia;
 CIEMAT, EELA, Ministerio de Educación y Ciencia of Spain, Xunta de Galicia (Consellería de Educación), CEADEN, Cubaenergía, Cuba, and IAEA (International Atomic Energy Agency);
 Swedish Research Council (VR) and Knut & Alice Wallenberg Foundation (KAW);
 Ukraine Ministry of Education and Science;
 United Kingdom Science and Technology Facilities Council (STFC);
 The United States Department of Energy, the United States National Science Foundation, the State of Texas, and the State of Ohio.

A The ALICE Collaboration

B. Abelev⁶⁹, A. Abrahantes Quintana⁶, D. Adamová⁷⁴, A.M. Adare¹²¹, M.M. Aggarwal⁷⁸,
 G. Aglieri Rinella³⁰, A.G. Agocs⁶⁰, A. Agostinelli¹⁹, S. Aguilar Salazar⁵⁶, Z. Ahammed¹¹⁷, N. Ahmad¹⁴,
 A. Ahmad Masoodi¹⁴, S.U. Ahn^{64,37}, A. Akindinov⁴⁶, D. Aleksandrov⁸⁹, B. Alessandro⁹⁵,
 R. Alfaro Molina⁵⁶, A. Alici^{96,30,9}, A. Alkin², E. Almaráz Aviña⁵⁶, T. Alt³⁶, V. Altini^{28,30}, S. Altinpinar¹⁵,
 I. Altsybeev¹¹⁸, C. Andrei⁷¹, A. Andronic⁸⁶, V. Anguelov⁸³, C. Anson¹⁶, T. Antičić⁸⁷, F. Antinori¹⁰⁰,
 P. Antonioli⁹⁶, L. Aphecetche¹⁰², H. Appelshäuser⁵², N. Arboř⁶⁵, S. Arce¹⁹, A. Arend⁵², N. Armesto¹³,
 R. Arnaldi⁹⁵, T. Aronsson¹²¹, I.C. Arsene⁸⁶, M. Arslanok⁵², A. Asryan¹¹⁸, A. Augustinus³⁰, R. Averbeck⁸⁶,
 T.C. Awes⁷⁵, J. Äystö³⁸, M.D. Azmi¹⁴, M. Bach³⁶, A. Badalá⁹⁷, Y.W. Baek^{64,37}, R. Bailhache⁵², R. Bala⁹⁵,
 R. Baldini Ferrolì⁹, A. Baldisseri¹², A. Baldit⁶⁴, F. Baltasar Dos Santos Pedrosa³⁰, J. Bán⁴⁷, R.C. Baral⁴⁸,
 R. Barbera²⁴, F. Barile²⁸, G.G. Barnaföldi⁶⁰, L.S. Barnby⁹¹, V. Barret⁶⁴, J. Bartke¹⁰⁵, M. Basile¹⁹, N. Bastid⁶⁴,
 B. Bathen⁵⁴, G. Batigne¹⁰², B. Batyunya⁵⁹, C. Baumann⁵², I.G. Bearden⁷², H. Beck⁵², I. Belikov⁵⁸,
 F. Bellini¹⁹, R. Bellwied¹¹¹, E. Belmont-Moreno⁵⁶, S. Beole²⁶, I. Berceanu⁷¹, A. Bercuci⁷¹, Y. Berdnikov⁷⁶,
 D. Berenyi⁶⁰, C. Bergmann⁵⁴, D. Berzano⁹⁵, L. Betev³⁰, A. Bhasin⁸¹, A.K. Bhati⁷⁸, L. Bianchi²⁶,
 N. Bianchi⁶⁶, C. Bianchin²², J. Bielčik³⁴, J. Bielčíková⁷⁴, A. Bilandžić⁷³, F. Blanco¹¹¹, F. Blanco⁷, D. Blau⁸⁹,
 C. Blume⁵², M. Boccioni³⁰, N. Bock¹⁶, A. Bogdanov⁷⁰, H. Bøggild⁷², M. Bogolyubsky⁴³, L. Boldizsár⁶⁰,

M. Bombara³⁵, J. Book⁵², H. Borel¹², A. Borissov¹²⁰, C. Bortolin^{22,ii}, S. Bose⁹⁰, F. Bossú^{30,26}, M. Botje⁷³,
 S. Böttger⁵¹, B. Boyer⁴², P. Braun-Munzinger⁸⁶, M. Bregant¹⁰², T. Breitner⁵¹, M. Broz³³, R. Brun³⁰,
 E. Bruna^{121,26,95}, G.E. Bruno²⁸, D. Budnikov⁸⁸, H. Buesching⁵², S. Bufalino^{26,95}, K. Bugaiev², O. Busch⁸³,
 Z. Buthelezi⁸⁰, D. Caffarri²², X. Cai⁴⁰, H. Caines¹²¹, E. Calvo Villar⁹², P. Camerini²⁰, V. Canoa Roman^{8,1},
 G. Cara Romeo⁹⁶, W. Carena³⁰, F. Carena³⁰, N. Carlin Filho¹⁰⁸, F. Carminati³⁰, C.A. Carrillo Montoya³⁰,
 A. Casanova Díaz⁶⁶, M. Caselle³⁰, J. Castillo Castellanos¹², J.F. Castillo Hernandez⁸⁶, E.A.R. Casula²¹,
 V. Catanescu⁷¹, C. Cavicchioli³⁰, J. Cepila³⁴, P. Cerello⁹⁵, B. Chang^{38,124}, S. Chapeland³⁰, J.L. Charvet¹²,
 S. Chattopadhyay¹¹⁷, S. Chattopadhyay⁹⁰, M. Cherney⁷⁷, C. Cheshkov^{30,110}, B. Cheynis¹¹⁰, E. Chiavassa⁹⁵,
 V. Chibante Barroso³⁰, D.D. Chinellato¹⁰⁹, P. Chochula³⁰, M. Chojnacki⁴⁵, P. Christakoglou^{73,45},
 C.H. Christensen⁷², P. Christiansen²⁹, T. Chujo¹¹⁵, S.U. Chung⁸⁵, C. Cicalo⁹³, L. Cifarelli^{19,30}, F. Cindolo⁹⁶,
 J. Cleymans⁸⁰, F. Coccetti⁹, J.-P. Coffin⁵⁸, F. Colamaria²⁸, D. Colella²⁸, G. Conesa Balbastre⁶⁵,
 Z. Conesa del Valle^{30,58}, P. Constantin⁸³, G. Contin²⁰, J.G. Contreras⁸, T.M. Cormier¹²⁰,
 Y. Corrales Morales²⁶, P. Cortese²⁷, I. Cortés Maldonado¹, M.R. Cosentino^{68,109}, F. Costa³⁰, M.E. Cotallo⁷,
 E. Crescio⁸, P. Crochet⁶⁴, E. Cruz Alaniz⁵⁶, E. Cuautle⁵⁵, L. Cunqueiro⁶⁶, A. Dainese^{22,100},
 H.H. Dalsgaard⁷², A. Danu⁵⁰, K. Das⁹⁰, D. Das⁹⁰, I. Das⁹⁰, S. Dash⁹⁵, A. Dash^{48,109}, S. De¹¹⁷,
 A. De Azevedo Moregula⁶⁶, G.O.V. de Barros¹⁰⁸, A. De Caro^{25,9}, G. de Cataldo⁹⁴, J. de Cuveland³⁶,
 A. De Falco²¹, D. De Gruttola²⁵, H. Delagrangé¹⁰², E. Del Castillo Sanchez³⁰, A. Deloff¹⁰¹, V. Demanov⁸⁸,
 N. De Marco⁹⁵, E. Dénes⁶⁰, S. De Pasquale²⁵, A. Deppman¹⁰⁸, G. D'Erasmus²⁸, R. de Rooij⁴⁵, D. Di Bari²⁸,
 T. Dietel⁵⁴, C. Di Giglio²⁸, S. Di Liberto⁹⁹, A. Di Mauro³⁰, P. Di Nezza⁶⁶, R. Divià³⁰, Ø. Djuvsland¹⁵,
 A. Dobrin^{120,29}, T. Dobrowolski¹⁰¹, I. Domínguez⁵⁵, B. Dönigus⁸⁶, O. Dordic¹⁸, O. Driga¹⁰², A.K. Dubey¹¹⁷,
 L. Ducroux¹¹⁰, P. Dupieux⁶⁴, A.K. Dutta Majumdar⁹⁰, M.R. Dutta Majumdar¹¹⁷, D. Elia⁹⁴,
 D. Emschermann⁵⁴, H. Engel⁵¹, H.A. Erdal³², B. Espagnon⁴², M. Estienne¹⁰², S. Esumi¹¹⁵, D. Evans⁹¹,
 G. Eyyubova¹⁸, D. Fabris^{22,100}, J. Faivre⁶⁵, D. Falchieri¹⁹, A. Fantoni⁶⁶, M. Fasel⁸⁶, R. Fearick⁸⁰,
 A. Fedunov⁵⁹, D. Fehler¹⁵, L. Feldkamp⁵⁴, D. Felea⁵⁰, G. Feofilov¹¹⁸, A. Fernández Téllez¹, A. Ferretti²⁶,
 R. Ferretti²⁷, J. Figiel¹⁰⁵, M.A.S. Figueredo¹⁰⁸, S. Filchagin⁸⁸, R. Fini⁹⁴, D. Finogeev⁴⁴, F.M. Fionda²⁸,
 E.M. Fiore²⁸, M. Floris³⁰, S. Foertsch⁸⁰, P. Foka⁸⁶, S. Fokin⁸⁹, E. Fragiaco⁹⁸, M. Fragkiadakis⁷⁹,
 U. Frankendorf⁸⁶, U. Fuchs³⁰, C. Furget⁶⁵, M. Fusco Girard²⁵, J.J. Gaardhøje⁷², M. Gagliardi²⁶, A. Gago⁹²,
 M. Gallio²⁶, D.R. Gangadharan¹⁶, P. Ganoti⁷⁵, C. Garabatos⁸⁶, E. Garcia-Solis¹⁰, I. Garishvili⁶⁹, J. Gerhard³⁶,
 M. Germain¹⁰², C. Geuna¹², M. Gheata³⁰, A. Gheata³⁰, B. Ghidini²⁸, P. Ghosh¹¹⁷, P. Gianotti⁶⁶,
 M.R. Girard¹¹⁹, P. Giubellino³⁰, E. Gladysz-Dziadus¹⁰⁵, P. Glässel⁸³, R. Gomez¹⁰⁷, E.G. Ferreira¹³,
 L.H. González-Trueba⁵⁶, P. González-Zamora⁷, S. Gorbunov³⁶, A. Goswami⁸², S. Gotovac¹⁰³, V. Grabski⁵⁶,
 L.K. Graczykowski¹¹⁹, R. Grajcarek⁸³, A. Grelli⁴⁵, C. Grigoras³⁰, A. Grigoras³⁰, V. Grigoriev⁷⁰,
 A. Grigoryan¹²², S. Grigoryan⁵⁹, B. Grinyov², N. Grion⁹⁸, P. Gros²⁹, J.F. Grosse-Oetringhaus³⁰,
 J.-Y. Grossiord¹¹⁰, R. Grosso³⁰, F. Guber⁴⁴, R. Guernane⁶⁵, C. Guerra Gutierrez⁹², B. Guerzoni¹⁹, M.
 Guilbaud¹¹⁰, K. Gulbrandsen⁷², T. Gunji¹¹⁴, A. Gupta⁸¹, R. Gupta⁸¹, H. Gutbrod⁸⁶, Ø. Haaland¹⁵,
 C. Hadjidakis⁴², M. Haiduc⁵⁰, H. Hamagaki¹¹⁴, G. Hamar⁶⁰, B.H. Han¹⁷, L.D. Hanratty⁹¹, A. Hansen⁷²,
 Z. Harmanova³⁵, J.W. Harris¹²¹, M. Hartig⁵², D. Hasegan⁵⁰, D. Hatzifotiadou⁹⁶, A. Hayrapetyan^{30,122},
 M. Heide⁵⁴, H. Helstrup³², A. Herghelegiu⁷¹, G. Herrera Corral⁸, N. Herrmann⁸³, K.F. Hetland³², B. Hicks¹²¹,
 P.T. Hille¹²¹, B. Hippolyte⁵⁸, T. Horaguchi¹¹⁵, Y. Hori¹¹⁴, P. Hristov³⁰, I. Hřivnáčová⁴², M. Huang¹⁵,
 S. Huber⁸⁶, T.J. Humanic¹⁶, D.S. Hwang¹⁷, R. Ichou⁶⁴, R. Ilkaev⁸⁸, I. Ilkiv¹⁰¹, M. Inaba¹¹⁵, E. Incani²¹,
 G.M. Innocenti²⁶, P.G. Innocenti³⁰, M. Ippolitov⁸⁹, M. Irfan¹⁴, C. Ivan⁸⁶, M. Ivanov⁸⁶, A. Ivanov¹¹⁸,
 V. Ivanov⁷⁶, O. Ivanytskyi², A. Jachořkowski³⁰, P. M. Jacobs⁶⁸, L. Jancurová⁵⁹, H.J. Jang⁶³, S. Jangal⁵⁸,
 R. Janik³³, M.A. Janik¹¹⁹, P.H.S.Y. Jayarathna¹¹¹, S. Jena⁴¹, R.T. Jimenez Bustamante⁵⁵, L. Jirde³⁰,
 P.G. Jones⁹¹, W. Jung³⁷, H. Jung³⁷, A. Jusko⁹¹, A.B. Kaidalov⁴⁶, V. Kakoyan¹²², S. Kalcher³⁶, P. Kaliňák⁴⁷,
 M. Kalisky⁵⁴, T. Kalliokoski³⁸, A. Kalweit⁵³, K. Kanaki¹⁵, J.H. Kang¹²⁴, V. Kaplin⁷⁰, A. Karasu Uysal^{30,123},
 O. Karavichev⁴⁴, T. Karavicheva⁴⁴, E. Karpechev⁴⁴, A. Kazantsev⁸⁹, U. Kebschull^{62,51}, R. Keidel¹²⁵,
 M.M. Khan¹⁴, P. Khan⁹⁰, S.A. Khan¹¹⁷, A. Khanzadeev⁷⁶, Y. Kharlov⁴³, B. Kileng³², D.W. Kim³⁷,
 M. Kim¹²⁴, J.H. Kim¹⁷, S.H. Kim³⁷, S. Kim¹⁷, B. Kim¹²⁴, T. Kim¹²⁴, D.J. Kim³⁸, J.S. Kim³⁷, S. Kirsch^{36,30},
 I. Kisel³⁶, S. Kiselev⁴⁶, A. Kisiel^{30,119}, J.L. Klay⁴, J. Klein⁸³, C. Klein-Bösing⁵⁴, M. Kliemant⁵², A. Kluge³⁰,
 M.L. Knichel⁸⁶, K. Koch⁸³, M.K. Köhler⁸⁶, A. Kolojvari¹¹⁸, V. Kondratiev¹¹⁸, N. Kondratyeva⁷⁰,
 A. Konevskikh⁴⁴, A. Korneev⁸⁸, C. Kottachchi Kankanamge Don¹²⁰, R. Kour⁹¹, M. Kowalski¹⁰⁵, S. Kox⁶⁵,
 G. Koyithatta Meethalevedu⁴¹, J. Kral³⁸, I. Králik⁴⁷, F. Kramer⁵², I. Kraus⁸⁶, T. Krawutschke^{83,31},
 M. Kretz³⁶, M. Krivda^{91,47}, F. Krizek³⁸, M. Krus³⁴, E. Kryshen⁷⁶, M. Krzewicki^{73,86}, Y. Kucheriaev⁸⁹,
 C. Kuhn⁵⁸, P.G. Kuijjer⁷³, P. Kurashvili¹⁰¹, A.B. Kurepin⁴⁴, A. Kurepin⁴⁴, A. Kuryakin⁸⁸, V. Kuschpil⁷⁴,
 S. Kuschpil⁷⁴, H. Kvaerno¹⁸, M.J. Kweon⁸³, Y. Kwon¹²⁴, P. Ladrón de Guevara⁵⁵, I. Lakomov¹¹⁸, R. Langoy¹⁵,
 C. Lara⁵¹, A. Lardeux¹⁰², P. La Rocca²⁴, C. Lazzeroni⁹¹, R. Lea²⁰, Y. Le Bornec⁴², K.S. Lee³⁷, S.C. Lee³⁷,

F. Lefèvre¹⁰², J. Lehnert⁵², L. Leistam³⁰, M. Lenhardt¹⁰², V. Lenti⁹⁴, H. León⁵⁶, I. León Monzón¹⁰⁷, H. León Vargas⁵², P. Lévai⁶⁰, X. Li¹¹, J. Lien¹⁵, R. Lietava⁹¹, S. Lindal¹⁸, V. Lindenstruth³⁶, C. Lippmann^{86,30}, M.A. Lisa¹⁶, L. Liu¹⁵, P.I. Loenne¹⁵, V.R. Loggins¹²⁰, V. Loginov⁷⁰, S. Lohn³⁰, D. Lohner⁸³, C. Loizides⁶⁸, K.K. Loo³⁸, X. Lopez⁶⁴, E. López Torres⁶, G. Løvhøiden¹⁸, X.-G. Lu⁸³, P. Luettig⁵², M. Lunardon²², J. Luo⁴⁰, G. Luparello⁴⁵, L. Luquin¹⁰², C. Luzzi³⁰, R. Ma¹²¹, K. Ma⁴⁰, D.M. Madagodahettige-Don¹¹¹, A. Maevskaya⁴⁴, M. Mager^{53,30}, D.P. Mahapatra⁴⁸, A. Maire⁵⁸, M. Malaev⁷⁶, I. Maldonado Cervantes⁵⁵, L. Malinina^{59,iii}, D. Mal'Kevich⁴⁶, P. Malzacher⁸⁶, A. Mamonov⁸⁸, L. Manceau⁹⁵, L. Mangotra⁸¹, V. Manko⁸⁹, F. Manso⁶⁴, V. Manzari⁹⁴, Y. Mao^{65,40}, M. Marchisone^{64,26}, J. Mares⁴⁹, G.V. Margagliotti^{20,98}, A. Margotti⁹⁶, A. Marín⁸⁶, C. Markert¹⁰⁶, I. Martashvili¹¹³, P. Martinengo³⁰, M.I. Martínez¹, A. Martínez Davalos⁵⁶, G. Martínez García¹⁰², Y. Martynov², A. Mas¹⁰², S. Masciocchi⁸⁶, M. Masera²⁶, A. Masoni⁹³, L. Massacrier¹¹⁰, M. Mastromarco⁹⁴, A. Mastroserio^{28,30}, Z.L. Matthews⁹¹, A. Matyja¹⁰², D. Mayani⁵⁵, C. Mayer¹⁰⁵, J. Mazer¹¹³, M.A. Mazzoni⁹⁹, F. Meddi²³, A. Menchaca-Rocha⁵⁶, J. Mercado Pérez⁸³, M. Meres³³, Y. Miake¹¹⁵, A. Michalon⁵⁸, J. Midori³⁹, L. Milano²⁶, J. Milosevic^{18,iv}, A. Mischke⁴⁵, A.N. Mishra⁸², D. Miśkowiec^{86,30}, C. Mitu⁵⁰, J. Mlynarz¹²⁰, A.K. Mohanty³⁰, B. Mohanty¹¹⁷, L. Molnar³⁰, L. Montaña Zetina⁸, M. Monteno⁹⁵, E. Montes⁷, T. Moon¹²⁴, M. Morando²², D.A. Moreira De Godoy¹⁰⁸, S. Moretto²², A. Morsch³⁰, V. Muccifora⁶⁶, E. Mudnic¹⁰³, S. Muhuri¹¹⁷, H. Müller³⁰, M.G. Munhoz¹⁰⁸, L. Musa³⁰, A. Musso⁹⁵, B.K. Nandi⁴¹, R. Nania⁹⁶, E. Nappi⁹⁴, C. Natrass¹¹³, N.P. Naumov⁸⁸, S. Navin⁹¹, T.K. Nayak¹¹⁷, S. Nazarenko⁸⁸, G. Nazarov⁸⁸, A. Nedosekin⁴⁶, M. Nicassio²⁸, B.S. Nielsen⁷², T. Niida¹¹⁵, S. Nikolaev⁸⁹, V. Nikolic⁸⁷, S. Nikulin⁸⁹, V. Nikulin⁷⁶, B.S. Nilsen⁷⁷, M.S. Nilsson¹⁸, F. Noferini^{96,9}, P. Nomokonov⁵⁹, G. Nooren⁴⁵, N. Novitzky³⁸, A. Nyanin⁸⁹, A. Nyatha⁴¹, C. Nygaard⁷², J. Nystrand¹⁵, H. Obayashi³⁹, A. Ochirov¹¹⁸, H. Oeschler^{53,30}, S.K. Oh³⁷, S. Oh¹²¹, J. Oleniacz¹¹⁹, C. Oppedisano⁹⁵, A. Ortiz Velasquez⁵⁵, G. Ortona^{30,26}, A. Oskarsson²⁹, P. Ostrowski¹¹⁹, I. Otterlund²⁹, J. Otwinowski⁸⁶, K. Oyama⁸³, K. Ozawa¹¹⁴, Y. Pachmayer⁸³, M. Pachr³⁴, F. Padilla²⁶, P. Pagano²⁵, G. Paic⁵⁵, F. Painke³⁶, C. Pajares¹³, S. Pal¹², S.K. Pal¹¹⁷, A. Palaha⁹¹, A. Palmeri⁹⁷, V. Papikyan¹²², G.S. Pappalardo⁹⁷, W.J. Park⁸⁶, A. Passfeld⁵⁴, B. Pastirčák⁴⁷, D.I. Patalakha⁴³, V. Patricchio⁹⁴, A. Pavlinov¹²⁰, T. Pawlak¹¹⁹, T. Peitzmann⁴⁵, M. Perales¹⁰, E. Pereira De Oliveira Filho¹⁰⁸, D. Peresunko⁸⁹, C.E. Pérez Lara⁷³, E. Perez Lezama⁵⁵, D. Perini³⁰, D. Perrino²⁸, W. Peryt¹¹⁹, A. Pesci⁹⁶, V. Peskov^{30,55}, Y. Pestov³, V. Petráček³⁴, M. Petran³⁴, M. Petris⁷¹, P. Petrov⁹¹, M. Petrovici⁷¹, C. Petta²⁴, S. Piano⁹⁸, A. Piccotti⁹⁵, M. Pikna³³, P. Pillot¹⁰², O. Pinazza³⁰, L. Pinsky¹¹¹, N. Pitz⁵², F. Piuze³⁰, D.B. Piyarathna¹¹¹, M. Płoskoń⁶⁸, J. Pluta¹¹⁹, T. Pocheptsov^{59,18}, S. Pochybova⁶⁰, P.L.M. Podesta-Lerma¹⁰⁷, M.G. Poghosyan^{30,26}, K. Polák⁴⁹, B. Polichtchouk⁴³, A. Pop⁷¹, S. Porteboeuf-Houssais⁶⁴, V. Pospíšil³⁴, B. Potukuchi⁸¹, S.K. Prasad¹²⁰, R. Preghenella^{96,9}, F. Prino⁹⁵, C.A. Pruneau¹²⁰, I. Pshenichnov⁴⁴, S. Puchagin⁸⁸, G. Puudu²¹, A. Pulvirenti^{24,30}, V. Punin⁸⁸, M. Putiš³⁵, J. Putschke^{120,121}, E. Quercigh³⁰, H. Qvigstad¹⁸, A. Rachevski⁹⁸, A. Rademakers³⁰, S. Radomski⁸³, T.S. Rähä³⁸, J. Rak³⁸, A. Rakotozafindrabe¹², L. Ramello²⁷, A. Ramírez Reyes⁸, R. Raniwala⁸², S. Raniwala⁸², S.S. Räsänen³⁸, B.T. Rascanu⁵², D. Rathee⁷⁸, K.F. Read¹¹³, J.S. Real⁶⁵, K. Redlich^{101,57}, P. Reichelt⁵², M. Reicher⁴⁵, R. Renfordt⁵², A.R. Reolon⁶⁶, A. Reshetin⁴⁴, F. Rettig³⁶, J.-P. Revol³⁰, K. Reygers⁸³, L. Riccati⁹⁵, R.A. Ricci⁶⁷, M. Richter¹⁸, P. Riedler³⁰, W. Riegler³⁰, F. Riggi^{24,97}, M. Rodríguez Cahuantzi¹, D. Rohr³⁶, D. Röhrich¹⁵, R. Romita⁸⁶, F. Ronchetti⁶⁶, P. Rosnet⁶⁴, S. Rossegger³⁰, A. Rossi²², F. Roukoutakis⁷⁹, C. Roy⁵⁸, P. Roy⁹⁰, A.J. Rubio Montero⁷, R. Rui²⁰, E. Ryabinkin⁸⁹, A. Rybicki¹⁰⁵, S. Sadovsky⁴³, K. Šafařík³⁰, P.K. Sahu⁴⁸, J. Saini¹¹⁷, H. Sakaguchi³⁹, S. Sakai⁶⁸, D. Sakata¹¹⁵, C.A. Salgado¹³, S. Sambyal⁸¹, V. Samsonov⁷⁶, X. Sanchez Castro⁵⁵, L. Šándor⁴⁷, A. Sandoval⁵⁶, M. Sano¹¹⁵, S. Sano¹¹⁴, R. Santo⁵⁴, R. Santoro^{94,30}, J. Sarkamo³⁸, E. Scapparone⁹⁶, F. Scarlassara²², R.P. Scharenberg⁸⁴, C. Schiaua⁷¹, R. Schicker⁸³, C. Schmidt⁸⁶, H.R. Schmidt^{86,116}, S. Schreiner³⁰, S. Schuchmann⁵², J. Schukraft³⁰, Y. Schutz^{30,102}, K. Schwarz⁸⁶, K. Schweda^{86,83}, G. Scioli¹⁹, E. Scomparin⁹⁵, P.A. Scott⁹¹, R. Scott¹¹³, G. Segato²², I. Selyuzhenkov⁸⁶, S. Senyukov^{27,58}, J. Seo⁸⁵, S. Serici²¹, E. Serradilla^{7,56}, A. Sevcenco⁵⁰, I. Sgura⁹⁴, A. Shabetai¹⁰², G. Shabratova⁵⁹, R. Shahoyan³⁰, N. Sharma⁷⁸, S. Sharma⁸¹, K. Shigaki³⁹, M. Shimomura¹¹⁵, K. Shtejer⁶, Y. Sibiraki⁸⁹, M. Siciliano²⁶, E. Sickling³⁰, S. Siddhanta⁹³, T. Siemiarczuk¹⁰¹, D. Silvermyr⁷⁵, G. Simonetti^{28,30}, R. Singaraju¹¹⁷, R. Singh⁸¹, S. Singha¹¹⁷, B.C. Sinha¹¹⁷, T. Sinha⁹⁰, B. Sitar³³, M. Sitta²⁷, T.B. Skaali¹⁸, K. Skjerdal¹⁵, R. Smakal³⁴, N. Smirnov¹²¹, R. Snellings⁴⁵, C. Søgaard⁷², R. Soltz⁶⁹, H. Son¹⁷, M. Song¹²⁴, J. Song⁸⁵, C. Soos³⁰, F. Soramel²², I. Sputowska¹⁰⁵, M. Spyropoulou-Stassinaki⁷⁹, B.K. Srivastava⁸⁴, J. Stachel⁸³, I. Stan⁵⁰, I. Stan⁵⁰, G. Stefanek¹⁰¹, G. Stefanini³⁰, T. Steinbeck³⁶, M. Steinpreis¹⁶, E. Stenlund²⁹, G. Steyn⁸⁰, D. Stocco¹⁰², M. Stolpovskiy⁴³, K. Strabykin⁸⁸, P. Strmen³³, A.A.P. Suaide¹⁰⁸, M.A. Subieta Vásquez²⁶, T. Sugitate³⁹, C. Suires⁴², M. Sukhorukov⁸⁸, R. Sultanov⁴⁶, M. Šumbera⁷⁴, T. Susa⁸⁷, A. Szanto de Toledo¹⁰⁸, I. Szarka³³, A. Szostak¹⁵, C. Tagridis⁷⁹, J. Takahashi¹⁰⁹, J.D. Tapia Takaki⁴², A. Tauro³⁰, G. Tejeda Muñoz¹, A. Telesca³⁰,

C. Terrevoli²⁸, J. Thäder⁸⁶, D. Thomas⁴⁵, J.H. Thomas⁸⁶, R. Tieulent¹¹⁰, A.R. Timmins¹¹¹, D. Tlusty³⁴, A. Toia^{36,30}, H. Torii^{39,114}, L. Toscano⁹⁵, F. Tosello⁹⁵, T. Traczyk¹¹⁹, D. Truesdale¹⁶, W.H. Trzaska³⁸, T. Tsuji¹¹⁴, A. Tumkin⁸⁸, R. Turrisi¹⁰⁰, T.S. Tsvetov¹⁸, J. Ulery⁵², K. Ullaland¹⁵, J. Ulrich^{62,51}, A. Uras¹¹⁰, J. Urbán³⁵, G.M. Urciuoli⁹⁹, G.L. Usai²¹, M. Vajzer^{34,74}, M. Vala^{59,47}, L. Valencia Palomo⁴², S. Vallero⁸³, N. van der Kolk⁷³, P. Vande Vyvre³⁰, M. van Leeuwen⁴⁵, L. Vannucci⁶⁷, A. Vargas¹, R. Varma⁴¹, M. Vasileiou⁷⁹, A. Vasiliev⁸⁹, V. Vechernin¹¹⁸, M. Veldhoen⁴⁵, M. Venaruzzo²⁰, E. Vercellin²⁶, S. Vergara¹, D.C. Vernekohl⁵⁴, R. Vernet⁵, M. Verweij⁴⁵, L. Vickovic¹⁰³, G. Viesti²², O. Vikhlyantsev⁸⁸, Z. Vilakazi⁸⁰, O. Villalobos Baillie⁹¹, L. Vinogradov¹¹⁸, A. Vinogradov⁸⁹, Y. Vinogradov⁸⁸, T. Virgili²⁵, Y.P. Viyogi¹¹⁷, A. Vodopyanov⁵⁹, S. Voloshin¹²⁰, K. Voloshin⁴⁶, G. Volpe^{28,30}, B. von Haller³⁰, D. Vranic⁸⁶, G. Øvrebeck¹⁵, J. Vrláková³⁵, B. Vulpescu⁶⁴, A. Vyushin⁸⁸, V. Wagner³⁴, B. Wagner¹⁵, R. Wan^{58,40}, Y. Wang⁸³, M. Wang⁴⁰, Y. Wang⁴⁰, D. Wang⁴⁰, K. Watanabe¹¹⁵, J.P. Wessels^{30,54}, U. Westerhoff⁵⁴, J. Wiechula^{83,116}, J. Wikne¹⁸, M. Wilde⁵⁴, A. Wilk⁵⁴, G. Wilk¹⁰¹, M.C.S. Williams⁹⁶, B. Windelband⁸³, L. Xaplanteris Karampatsos¹⁰⁶, S. Yang¹⁵, H. Yang¹², S. Yano³⁹, S. Yasnopolskiy⁸⁹, J. Yi⁸⁵, Z. Yin⁴⁰, H. Yokoyama¹¹⁵, I.-K. Yoo⁸⁵, J. Yoon¹²⁴, W. Yu⁵², X. Yuan⁴⁰, I. Yushmanov⁸⁹, C. Zach³⁴, C. Zampolli^{96,30}, S. Zaporozhets⁵⁹, A. Zarochentsev¹¹⁸, P. Závada⁴⁹, N. Zaviyalov⁸⁸, H. Zbroszczyk¹¹⁹, P. Zelnicsek^{30,51}, I. Zgura⁵⁰, M. Zhalov⁷⁶, X. Zhang^{64,40}, D. Zhou⁴⁰, Y. Zhou⁴⁵, F. Zhou⁴⁰, X. Zhu⁴⁰, A. Zichichi^{19,9}, A. Zimmermann⁸³, G. Zinovjev², Y. Zoccarato¹¹⁰, M. Zynovyev²

Affiliation notes

ⁱ Deceased

ⁱⁱ Also at: Dipartimento di Fisica dell'Università, Udine, Italy

ⁱⁱⁱ Also at: M.V.Lomonosov Moscow State University, D.V.Skobeltzyn Institute of Nuclear Physics, Moscow, Russia

^{iv} Also at: "Vinča" Institute of Nuclear Sciences, Belgrade, Serbia

Collaboration Institutes

¹ Benemérita Universidad Autónoma de Puebla, Puebla, Mexico

² Bogolyubov Institute for Theoretical Physics, Kiev, Ukraine

³ Budker Institute for Nuclear Physics, Novosibirsk, Russia

⁴ California Polytechnic State University, San Luis Obispo, California, United States

⁵ Centre de Calcul de l'IN2P3, Villeurbanne, France

⁶ Centro de Aplicaciones Tecnológicas y Desarrollo Nuclear (CEADEN), Havana, Cuba

⁷ Centro de Investigaciones Energéticas Medioambientales y Tecnológicas (CIEMAT), Madrid, Spain

⁸ Centro de Investigación y de Estudios Avanzados (CINVESTAV), Mexico City and Mérida, Mexico

⁹ Centro Fermi – Centro Studi e Ricerche e Museo Storico della Fisica "Enrico Fermi", Rome, Italy

¹⁰ Chicago State University, Chicago, United States

¹¹ China Institute of Atomic Energy, Beijing, China

¹² Commissariat à l'Énergie Atomique, IRFU, Saclay, France

¹³ Departamento de Física de Partículas and IGFAE, Universidad de Santiago de Compostela, Santiago de Compostela, Spain

¹⁴ Department of Physics Aligarh Muslim University, Aligarh, India

¹⁵ Department of Physics and Technology, University of Bergen, Bergen, Norway

¹⁶ Department of Physics, Ohio State University, Columbus, Ohio, United States

¹⁷ Department of Physics, Sejong University, Seoul, South Korea

¹⁸ Department of Physics, University of Oslo, Oslo, Norway

¹⁹ Dipartimento di Fisica dell'Università and Sezione INFN, Bologna, Italy

²⁰ Dipartimento di Fisica dell'Università and Sezione INFN, Trieste, Italy

²¹ Dipartimento di Fisica dell'Università and Sezione INFN, Cagliari, Italy

²² Dipartimento di Fisica dell'Università and Sezione INFN, Padova, Italy

²³ Dipartimento di Fisica dell'Università 'La Sapienza' and Sezione INFN, Rome, Italy

²⁴ Dipartimento di Fisica e Astronomia dell'Università and Sezione INFN, Catania, Italy

²⁵ Dipartimento di Fisica 'E.R. Caianiello' dell'Università and Gruppo Collegato INFN, Salerno, Italy

²⁶ Dipartimento di Fisica Sperimentale dell'Università and Sezione INFN, Turin, Italy

²⁷ Dipartimento di Scienze e Tecnologie Avanzate dell'Università del Piemonte Orientale and Gruppo Collegato INFN, Alessandria, Italy

- 28 Dipartimento Interateneo di Fisica ‘M. Merlin’ and Sezione INFN, Bari, Italy
- 29 Division of Experimental High Energy Physics, University of Lund, Lund, Sweden
- 30 European Organization for Nuclear Research (CERN), Geneva, Switzerland
- 31 Fachhochschule Köln, Köln, Germany
- 32 Faculty of Engineering, Bergen University College, Bergen, Norway
- 33 Faculty of Mathematics, Physics and Informatics, Comenius University, Bratislava, Slovakia
- 34 Faculty of Nuclear Sciences and Physical Engineering, Czech Technical University in Prague, Prague, Czech Republic
- 35 Faculty of Science, P.J. Šafárik University, Košice, Slovakia
- 36 Frankfurt Institute for Advanced Studies, Johann Wolfgang Goethe-Universität Frankfurt, Frankfurt, Germany
- 37 Gangneung-Wonju National University, Gangneung, South Korea
- 38 Helsinki Institute of Physics (HIP) and University of Jyväskylä, Jyväskylä, Finland
- 39 Hiroshima University, Hiroshima, Japan
- 40 Hua-Zhong Normal University, Wuhan, China
- 41 Indian Institute of Technology, Mumbai, India
- 42 Institut de Physique Nucléaire d’Orsay (IPNO), Université Paris-Sud, CNRS-IN2P3, Orsay, France
- 43 Institute for High Energy Physics, Protvino, Russia
- 44 Institute for Nuclear Research, Academy of Sciences, Moscow, Russia
- 45 Nikhef, National Institute for Subatomic Physics and Institute for Subatomic Physics of Utrecht University, Utrecht, Netherlands
- 46 Institute for Theoretical and Experimental Physics, Moscow, Russia
- 47 Institute of Experimental Physics, Slovak Academy of Sciences, Košice, Slovakia
- 48 Institute of Physics, Bhubaneswar, India
- 49 Institute of Physics, Academy of Sciences of the Czech Republic, Prague, Czech Republic
- 50 Institute of Space Sciences (ISS), Bucharest, Romania
- 51 Institut für Informatik, Johann Wolfgang Goethe-Universität Frankfurt, Frankfurt, Germany
- 52 Institut für Kernphysik, Johann Wolfgang Goethe-Universität Frankfurt, Frankfurt, Germany
- 53 Institut für Kernphysik, Technische Universität Darmstadt, Darmstadt, Germany
- 54 Institut für Kernphysik, Westfälische Wilhelms-Universität Münster, Münster, Germany
- 55 Instituto de Ciencias Nucleares, Universidad Nacional Autónoma de México, Mexico City, Mexico
- 56 Instituto de Física, Universidad Nacional Autónoma de México, Mexico City, Mexico
- 57 Institut of Theoretical Physics, University of Wrocław
- 58 Institut Pluridisciplinaire Hubert Curien (IPHC), Université de Strasbourg, CNRS-IN2P3, Strasbourg, France
- 59 Joint Institute for Nuclear Research (JINR), Dubna, Russia
- 60 KFKI Research Institute for Particle and Nuclear Physics, Hungarian Academy of Sciences, Budapest, Hungary
- 61 Kharkiv Institute of Physics and Technology (KIPT), National Academy of Sciences of Ukraine (NASU), Kharkov, Ukraine
- 62 Kirchhoff-Institut für Physik, Ruprecht-Karls-Universität Heidelberg, Heidelberg, Germany
- 63 Korea Institute of Science and Technology Information
- 64 Laboratoire de Physique Corpusculaire (LPC), Clermont Université, Université Blaise Pascal, CNRS-IN2P3, Clermont-Ferrand, France
- 65 Laboratoire de Physique Subatomique et de Cosmologie (LPSC), Université Joseph Fourier, CNRS-IN2P3, Institut Polytechnique de Grenoble, Grenoble, France
- 66 Laboratori Nazionali di Frascati, INFN, Frascati, Italy
- 67 Laboratori Nazionali di Legnaro, INFN, Legnaro, Italy
- 68 Lawrence Berkeley National Laboratory, Berkeley, California, United States
- 69 Lawrence Livermore National Laboratory, Livermore, California, United States
- 70 Moscow Engineering Physics Institute, Moscow, Russia
- 71 National Institute for Physics and Nuclear Engineering, Bucharest, Romania
- 72 Niels Bohr Institute, University of Copenhagen, Copenhagen, Denmark
- 73 Nikhef, National Institute for Subatomic Physics, Amsterdam, Netherlands
- 74 Nuclear Physics Institute, Academy of Sciences of the Czech Republic, Řež u Prahy, Czech Republic
- 75 Oak Ridge National Laboratory, Oak Ridge, Tennessee, United States

- 76 Petersburg Nuclear Physics Institute, Gatchina, Russia
- 77 Physics Department, Creighton University, Omaha, Nebraska, United States
- 78 Physics Department, Panjab University, Chandigarh, India
- 79 Physics Department, University of Athens, Athens, Greece
- 80 Physics Department, University of Cape Town, iThemba LABS, Cape Town, South Africa
- 81 Physics Department, University of Jammu, Jammu, India
- 82 Physics Department, University of Rajasthan, Jaipur, India
- 83 Physikalisches Institut, Ruprecht-Karls-Universität Heidelberg, Heidelberg, Germany
- 84 Purdue University, West Lafayette, Indiana, United States
- 85 Pusan National University, Pusan, South Korea
- 86 Research Division and ExtreMe Matter Institute EMMI, GSI Helmholtzzentrum für Schwerionenforschung, Darmstadt, Germany
- 87 Rudjer Bošković Institute, Zagreb, Croatia
- 88 Russian Federal Nuclear Center (VNIIEF), Sarov, Russia
- 89 Russian Research Centre Kurchatov Institute, Moscow, Russia
- 90 Saha Institute of Nuclear Physics, Kolkata, India
- 91 School of Physics and Astronomy, University of Birmingham, Birmingham, United Kingdom
- 92 Sección Física, Departamento de Ciencias, Pontificia Universidad Católica del Perú, Lima, Peru
- 93 Sezione INFN, Cagliari, Italy
- 94 Sezione INFN, Bari, Italy
- 95 Sezione INFN, Turin, Italy
- 96 Sezione INFN, Bologna, Italy
- 97 Sezione INFN, Catania, Italy
- 98 Sezione INFN, Trieste, Italy
- 99 Sezione INFN, Rome, Italy
- 100 Sezione INFN, Padova, Italy
- 101 Soltan Institute for Nuclear Studies, Warsaw, Poland
- 102 SUBATECH, Ecole des Mines de Nantes, Université de Nantes, CNRS-IN2P3, Nantes, France
- 103 Technical University of Split FESB, Split, Croatia
- 104 test institute
- 105 The Henryk Niewodniczanski Institute of Nuclear Physics, Polish Academy of Sciences, Cracow, Poland
- 106 The University of Texas at Austin, Physics Department, Austin, TX, United States
- 107 Universidad Autónoma de Sinaloa, Culiacán, Mexico
- 108 Universidade de São Paulo (USP), São Paulo, Brazil
- 109 Universidade Estadual de Campinas (UNICAMP), Campinas, Brazil
- 110 Université de Lyon, Université Lyon 1, CNRS/IN2P3, IPN-Lyon, Villeurbanne, France
- 111 University of Houston, Houston, Texas, United States
- 112 University of Technology and Austrian Academy of Sciences, Vienna, Austria
- 113 University of Tennessee, Knoxville, Tennessee, United States
- 114 University of Tokyo, Tokyo, Japan
- 115 University of Tsukuba, Tsukuba, Japan
- 116 Eberhard Karls Universität Tübingen, Tübingen, Germany
- 117 Variable Energy Cyclotron Centre, Kolkata, India
- 118 V. Fock Institute for Physics, St. Petersburg State University, St. Petersburg, Russia
- 119 Warsaw University of Technology, Warsaw, Poland
- 120 Wayne State University, Detroit, Michigan, United States
- 121 Yale University, New Haven, Connecticut, United States
- 122 Yerevan Physics Institute, Yerevan, Armenia
- 123 Yildiz Technical University, Istanbul, Turkey
- 124 Yonsei University, Seoul, South Korea
- 125 Zentrum für Technologietransfer und Telekommunikation (ZTT), Fachhochschule Worms, Worms, Germany